Model system for optical nonlinearities: Asymmetric quantum wells

E. Rosencher and Ph. Bois
Laboratoire Central de Recherches, Thomson–CSF, F-91404 Orsay CEDEX, France
(Received 23 May 1991)

Optical nonlinearities in asymmetric quantum wells due to resonant intersubband transitions are analyzed using a compact density-matrix approach. The large dipolar matrix elements obtained in such structures are partly due to the small effective masses of the host materials and are interpreted in terms of the participation of the whole band structure to the optical transitions. The other origin of the large second-order susceptibilities lies in the possibility of tuning independently the potential shape and the width of asymmetric quantum wells in order to obtain resonances (single or double) for a given excitation wavelength. Using a model based on an infinite-barrier quantum well, we have obtained very general and tractable formulas for second-order susceptibilities at resonance. This model allows us to fix additional fundamental quantum limitations to second-order optical nonlinearities. The "best potential shapes" maximizing the different susceptibilities are obtained, together with *scaling laws* as a function of photon energy. Experimental results on different GaAs/$Al_xGa_{1-x}As$ asymmetric quantum wells optimized for second-harmonic generation and optical rectifications are given, with optical rectification coefficients more than 10^6 higher than in bulk GaAs. These asymmetric quantum wells may be considered as giant "pseudomolecules" optimized for large optical nonlinearities in the 8–12-μm range.

I. INTRODUCTION

Thanks to the recent progress in epitaxy techniques, it is now possible to grow alternating layers of semiconductors with different band-gap energies with a thickness control down to one atomic layer. It is now well established that these systems behave, as far as the electron motion is concerned, as a succession of potential barriers and wells. If the width of the potential well is less than the de Broglie wavelength of the electrons in the material (e.g., less than ≈ 15 nm in GaAs), the motion of the electrons may be considered, at sufficiently low temperature, as quantized in the direction normal to the growth axis.[1] The electrons are quantized into subbands where their wave functions in the growth direction have the form of envelope functions with an extension equal to the well width, i.e., in the few-nanometer range. Electromagnetic waves may induce electronic transitions between these subbands. The dipole matrix elements associated to these intersubband transitions (ISBT) have the same order of magnitude as the quantum-well width leading to extremely large absorption. These large absorptions have been observed in GaAs/$Al_xGa_{1-x}As$ multiple quantum wells (MQW's) by West and Eglash[2] and subsequently used by Levine *et al.*[3] in a class of infrared photoconductive detectors.

The dipole matrix elements are thus in the few-nanometer range instead of the few picometers obtained in usual molecular or ionic systems.[4] Since second-order optical susceptibilities have a cubic dependence relative to the dipole matrix elements, strong second-order optical nonlinearities are expected in MQW's insofar as inversion symmetry is broken. In their pioneering work, Gurnick and DeTemple have suggested obtaining this asymmetry by growing $Al_xGa_{1-x}As$ MQW's with asymmetric composition gradients of Al in the growth direction.[5] In their paper, these authors have consider an asymmetric Morse potential and have shown that nonlinearities of 10 to 100 times larger than in bulk materials could be theoretically possible. Kurghin later suggested using asymmetric coupled quantum wells.[6] Ahn and Chuang proposed to bias a symmetric QW electrically to obtain this asymmetry.[7] This has been realized by Fejer *et al.* who obtained a second-harmonic-generation coefficient more than 70 times higher than in bulk GaAs.[8] In a more recent work, Yuh and Wang suggested that the use of a step-quantum-well (QW) structure, which consists of a small well inside a bigger one, would be easier to fabricate and could yield also large second-harmonic nonlinearities.[9] Rosencher *et al.* have shown that these step QW's could be designed so that the absorption could be doubly resonant, leading to second-harmonic-generation (SHG) coefficients more than three orders of magnitude higher than in bulk GaAs.[10] These latter authors have realized different step QW's and observed indeed extremely large second-order optical nonlinearities (SHG, optical rectification).[11–14] These huge nonlinearities in step QW's have been confirmed by Karunasiri, Mii, and Wang, who measured linear Stark effects as high as 0.44 meV cm/kV.[15]

The purposes of this paper are the following. In Sec. II, we shall discuss in some detail the physical origin of the large dipole moments of ISBT in GaAs quantum wells. In particular, we will show that these large oscillator strengths originate from the contribution of the optical transitions between the conduction band and all the other bands of the crystal structure. In Sec. III, we will present a compact description of the density-matrix formalism which leads to simple expressions of second-order susceptibilities in QW's, without resorting to general,

complete, and cumbersome formulations of optical nonlinearities. This description leads to particularly simple and illustrative formulas for the various effects. The second-order nonlinearity coefficients are found to be proportional to the product of overlapping integrals between the envelope wave functions of the different subbands. *Applying this formalism to step quantum wells considered as a physical model for resonant optical nonlinearities, one may thus analyze optical nonlinearities in terms of purely geometrical factors and thus fix additional fundamental quantum limitations to second-order susceptibilities,* which is described in Sec. IV. These scaling rules are different from preceding ones, such as those of Flytzanis[16] or Oudar and Zyss,[17] in that in our approach only resonant transitions are envisioned and mostly geometrical considerations are involved. In Sec. V, we will give our experimental results on different asymmetric QW's optimized for second-harmonic generation and optical rectification. We will show that these asymmetric QW's (AQW's) behave as giant "pseudomolecules" optimized for large optical nonlinearities in the 8–12-μm range.

II. EFFECTIVE-MASS EFFECT ON THE OSCILLATOR STRENGTHS IN INTERSUBBAND TRANSITIONS

In this section, we will mostly focus on the eigenfunctions involved in ISBT and will analyze in some detail the connections between the oscillator strengths and the effective mass. Electrons in a semiconductor quantum well are particularly well described by the effective-mass Hamiltonian[18]

$$H=-\frac{\hbar^2}{2m^*}\left[\frac{\delta^2}{\delta x^2}+\frac{\delta^2}{\delta y^2}+\frac{\delta^2}{\delta z^2}\right]+V(z)\ , \tag{1}$$

where z represents the growth direction, $\hbar$ is Planck's constant, and $V(z)$ is the profile of the conduction-band potential in the quantum well. The conduction-band effective mass m^* will be taken constant in the rest of the paper, i.e., we neglect band nonparabolicity for the sake of simplicity. Moreover, screening effects due to the doping of the QW's and the electron gas itself are neglected in this approach. In particular, it means that the plasmon shift (in the few meV for usual doping concentration) of the optical resonances is not taken into account[19] and that the electrostatic screening length in the quantum well is assumed large compared to the QW thickness, which is reasonable.[20] The eigenfunctions $\Psi_{n,k}(\mathbf{r})$ and the eigenenergies e_n are solutions of the Schrödinger equation $H\Psi_{n,\mathbf{k}}(\mathbf{r})=e_{n,\mathbf{k}}\Psi_{n,\mathbf{k}}(\mathbf{r})$ and are given by

$$\Psi_{n,\mathbf{k}}(\mathbf{r})=\zeta_n(z)u_c(\mathbf{r})e^{i\mathbf{k}_\parallel\cdot\mathbf{r}_\parallel} \tag{2}$$

and

$$e_{n,\mathbf{k}}=E_n+\frac{\hbar^2}{2m^*}|\mathbf{k}_\parallel|^2\ . \tag{3}$$

Here, $\mathbf{k}_\parallel$ and $\mathbf{r}_\parallel$ are the wave vector and coordinate in the xy plane and $u_c(\mathbf{r})$ is the periodic part of the Bloch function in the conduction band at $k=0$. ζ_n and E_n are, respectively, the envelope wave function and the transverse energy of the nth subband, solutions of the one-dimensional Schrödinger equation $H_0\zeta_n(z)=E_n\zeta_n(z)$, where H_0 is the z part of the Hamiltonian H in Eq. (1), i.e., $H_0=\hbar^2/2m^*d^2/dz^2+V(z)$. The subband energy dispersion curves are given in Eq. (3).

If the structure is doped, at sufficiently low temperature most of the electrons are located in the first subband e_1. Let us consider an electromagnetic field of frequency ω which is incident with a polarization vector normal to the quantum wells. The dipolar interaction is given by $qE_0z\cos\omega t$, where q is the electronic charge. Time-dependent perturbation theory shows that the electrons are then in the steady state:[21]

$$|\psi(t)\rangle=|\psi_1\rangle+\sum_{n(\neq 1)}\frac{qE_0}{2\hbar}\langle\psi_n|z|\psi_1\rangle\frac{e^{-i\omega t}}{(\omega_{1n}-\omega)+\frac{\hbar^2}{2m^*}|\mathbf{k}_\parallel^n-\mathbf{k}_\parallel^1|^2+i\Gamma_{n1}}|\psi_n\rangle\ , \tag{4}$$

where $\omega_{1n}=E_{1n}/\hbar=(E_n-E_1)/\hbar$ is Bohr's frequency, and $\mathbf{k}_\parallel^n$ and $\mathbf{k}_\parallel^1$ are the parallel wave vectors in subbands n and 1, respectively. We have made the near-resonant approximation [neglecting the $(\omega+\omega_{1n})$ terms] and neglected transient behavior ($\exp\pm i\omega_{1n}t$ terms) by introducing the lifetimes Γ_{n1}. Symmetry considerations on Bloch states show that[1]

$$\langle\psi_n|z|\psi_1\rangle=\delta_{\mathbf{k}_\parallel^n,\mathbf{k}_\parallel^1}\langle\zeta_n|z|\zeta_1\rangle\ , \tag{5}$$

where δ is the Kronecker function. The mean value of the polarization per unit surface observable $P=qz$ per QW is given by $P(t)=\rho_s\langle\Psi(t)|qz|\Psi(t)\rangle$, where ρ_s is the surface density of carriers in the QW. The quadrature phase term $P_A(t)$ is then

$$P_A(t)=\frac{q^2E_0\rho_s}{\hbar}\sum_{n(\neq 1)}\frac{\Gamma_{1n}|\langle\zeta_n|z|\zeta_1\rangle|^2}{(\omega_{1n}-\omega)^2+\Gamma_{1n}^2}\sin(\omega t)\ . \tag{6}$$

By identification, this leads to the expression of the absorption coefficient per well α:[22]

$$\alpha=\frac{q^2\pi\rho_s}{2m^*n\epsilon_0c}\sum_{n(\neq 1)}f_{1n}\frac{\omega}{\omega_{1n}}\frac{\Gamma_{1n}/\pi}{(\omega_{1n}-\omega)^2+\Gamma_{1n}^2}\ , \tag{7}$$

where ϵ_0 is the vacuum permittivity, c is the speed of light, n is the dielectric constant of the material, and f_{1n} is the usual oscillator strength given by

$$f_{1n}=\frac{2m^*}{\hbar^2}E_{1n}|\langle\zeta_n|z|\zeta_1\rangle|^2\ . \tag{8}$$

The integrated absorption on the nth peak, $A_I(n)$, which is the percentage of light power absorbed in the QW by the nth resonance, is

$$A_I(n)=\int_{n\text{th peak}}\alpha(\omega)d\omega=\frac{q^2\pi\rho_s}{2m^*n\epsilon_0 c}f_{1n} . \tag{9}$$

At this stage, it is important to note that, since the commutation rules $[z,p_z]=i\hbar$ and $[H_0,z]=-i\hbar p_z/m^*$ apply to our system, the oscillator strengths given by Eq. (8) respect the Thomas-Reich-Kuhn sum rule

$$\sum_{n(\neq 1)} f_{1n}=1 \tag{10}$$

so that

$$A_T^*=\sum_{n(\neq 1)} A_I(n)=\frac{q^2\pi\rho_s}{2m_0 n\epsilon_0 c}\frac{m_0}{m^*} , \tag{11}$$

where A_T^* is the total absorption from E_1 on the whole spectrum and m_0 is the free-electron mass. The total absorption is thus a factor m_0/m^* higher in QW's (i.e., 14.9 in GaAs) than in a bulk material (or a system with $m^*=m_0$ such as a molecule). This remark is the key point that leads to giant optical nonlinearities. We derive a very crude but illustrating argument of this phenomenon below.

Indeed, we may simplify Eq. (10) by noting that, in intersubband transitions, most of the oscillator strength is located in the $1\rightarrow 2$ transition ($f_{12}\approx 0.96$ for an infinitely deep potential well), i.e., $f_{12}\approx 1$. This reads

$$\frac{2m^*}{\hbar^2}E_{12}\mu_{12}^2\approx 1 , \tag{12}$$

where $\mu_{ij}=|\langle\xi_j|z|\xi_i\rangle|$ is the off-diagonal matrix element. Since μ_{12} has the same order of magnitude as the QW width L, Eq. (12) is merely the approximate energy solution of the Schrödinger equation of an infinitely deep QW. Equation (12) thus stipulates that, *for a given photon energy E_{12}, the dipole matrix element will be $(m_0/m^*)^{1/2}$ higher in quantum wells than in molecules.* Quantum wells behave, as far as intersubband transitions are concerned, as giant "pseudomolecules."

One may look for a first-principles origin of these large dipole elements in the crystal structure of the host material. The difference between the total absorption A_T for an $m^*=m_0$ material and A_T^* is

$$A_T^*-A_T=C\left[\frac{m_0}{m^*}-1\right] , \tag{13}$$

where C is a constant given by Eq. (11). Using the $\mathbf{k}\cdot\mathbf{p}$ formalism,[23] Eq. (13) yields

$$A_T^*-A_T=C\frac{2m_0}{\hbar^2}\sum_{j(\neq c)}(E_{c,\mathbf{k}=0}-E_{j,\mathbf{k}=0})\times|\langle u_{j,\mathbf{k}=0}|z|u_{c,\mathbf{k}=0}\rangle|^2 , \tag{14}$$

where j denotes the band index, $E_{j,\mathbf{k}=0}$ indicates the extrema of the different bands at $\mathbf{k}=\mathbf{0}$ in the band structure, and c is the index corresponding to the conduction band. This latter formulation means that *the enhancement of the total absorption originates from the contribution of the optical transitions between the conduction band and the other bands of the crystal structure.* This is of course at the expense of other oscillator strength involved in other optical transitions since the sum of the oscillator strengths over the entire band structure must eventually be equal to 1.

III. NONLINEAR OPTICAL SUSCEPTIBILITIES FROM THE DENSITY-MATRIX FORMALISM

In this section, we will present a compact formalism for the derivation of second-order nonlinearities in AMQW's. Special emphasis will be put on optical rectification and the electro-optic effect, this aspect being rarely addressed in the literature. Let us consider the system described by the Hamiltonian H_0 of Sec. II. At thermal equilibrium, the density matrix $\rho^{(0)}$ is a diagonal one, in which the diagonal elements $\rho_{ii}^{(0)}$ are the surface thermal population ρ_i of level E_i given by the Fermi level in the QW. The system is excited by an internal electromagnetic field

$$E(t)=\tilde{E}e^{i\omega t}+\tilde{E}e^{-i\omega t} . \tag{15}$$

The evolution of the density matrix is given by the time-dependent Schrödinger equation

$$\frac{\partial\rho_{ij}}{\partial t}=\frac{1}{i\hbar}[H_0-qzE(t),\rho]_{ij}-\Gamma_{ij}(\rho-\rho^{(0)})_{ij} . \tag{16}$$

For simplicity, we will assume in the following only two different values of the relaxation rates: $\Gamma_1=1/T_1$ for $i=j$ is the diagonal (or inelastic) relaxation rate and $\Gamma_2=1/T_2$ is the off-diagonal (or elastic) relaxation rate. Equation (16) is solved using the usual iterative method:[4,7]

$$\rho(t)=\sum_n\rho^{(n)}(t) \tag{17}$$

with

$$\frac{\partial\rho_{ij}^{(n+1)}}{\partial t}=\frac{1}{i\hbar}\{[H_0,\rho^{(n+1)}]_{ij}-i\hbar\Gamma_{ij}\rho_{ij}^{(n+1)}\}-\frac{1}{i\hbar}[qz,\rho^{(n)}]_{ij}E(t) . \tag{18}$$

The electronic polarization of the QW will also be a series expansion as Eq. (17). We shall limit ourselves to the first two orders, i.e.,

$$P(t)=(\epsilon_0\chi^{(1)}\tilde{E}e^{i\omega t}+\epsilon_0\chi_{2\omega}^{(2)}\tilde{E}^2e^{2i\omega t})+\text{c.c.}+\epsilon_0\chi_0^{(2)}\tilde{E}^2 , \tag{19}$$

where $\chi^{(1)}$, $\chi_{2\omega}^{(2)}$, and $\chi_0^{(2)}$ are the linear, second-harmonic generation, and optical rectification coefficients, respectively. The electronic polarization of the nth order is given by

$$P^{(n)}(t)=\frac{1}{S}\text{Tr}(\rho^{(n)}qz) , \tag{20}$$

where S is the area of interaction.

We will treat two cases in the following: (i) The optical

rectification in a two-level system: two levels are indeed enough to guarantee the double-resonance effect ($\omega-\omega=0$); and (ii) the second-harmonic generation in a system with three levels that are equally spaced in energy in order to guarantee double-resonance effects ($\omega+\omega=2\omega$).

A. Optical rectification in a two-level system

The application of Eq. (18) to $n=0$ yields

$$\rho^{(1)}(t)=\tilde{\rho}^{(1)}(\omega)e^{i\omega t}+\tilde{\rho}^{(1)}(-\omega)e^{-i\omega t} \tag{21}$$

with

$$\tilde{\rho}_{ij}^{(1)}-\frac{q\mu_{ij}(n_j-n_i)}{\hbar[(\omega+\omega_{ji})-i\Gamma_{ij}]}\tilde{E} \ . \tag{22}$$

The application of Eq. (20) leads directly to the expression of the absorption coefficient, which is identical to Eq. (9) apart from ρ_s being replaced by $(\rho_1-\rho_2)$, where $\rho_i=n_i/S$ is the surface concentration of carriers in the ith subband. The next iteration ($n=1$) leads to

$$\rho^{(2)}(t)=\tilde{\rho}_{2\omega}^{(2)}(\omega)e^{2i\omega t}+\tilde{\rho}_{2\omega}^{(2)}(-\omega)e^{-2i\omega t}+R^{(2)} \ , \tag{23}$$

where $R^{(2)}$ is the time constant density matrix associated with optical rectification (OR), solution of

$$[H_0,R^{(2)}]_{ij}-i\Gamma_{ij}R_{ij}^{(2)}=[qz,\tilde{\rho}^{(1)}(\omega)+\tilde{\rho}^{(1)}(-\omega)]_{ij}\tilde{E} \ . \tag{24}$$

The elements of $R^{(2)}$ are thus

$$R_{22}^{(2)}=-R_{11}^{(2)}=2\frac{q^2\mu_{12}^2(n_1-n_2)}{\hbar^2}\tilde{E}^2\frac{\Gamma_2}{\Gamma_1}\times\left[\frac{1}{(\omega_{12}-\omega)^2+\Gamma_2^2}+\frac{1}{(\omega_{12}+\omega)^2+\Gamma_2^2}\right] \tag{25}$$

and

$$R_{12}^{(2)}=\frac{q^2\delta_{12}\mu_{12}(n_1-n_2)}{\hbar^2}\tilde{E}^2\frac{1}{\omega_{12}+i\Gamma_2}\times\left[\frac{1}{(\omega-\omega_{12})-i\Gamma_2}-\frac{1}{(\omega+\omega_{12})+i\Gamma_2}\right], \tag{25'}$$

where $\delta_{12}=\langle\zeta_2|z|\zeta_2\rangle-\langle\zeta_1|z|\zeta_1\rangle$ is the mean electron displacement during the transition. $R_{21}^{(2)}$ is given by the commutation of indexes 1 and 2 in Eq. (25'). By using Eqs. (19), (20), and (25), one finally finds the OR coefficient per unit surface:

$$\chi_0^{(2)}=4\frac{q^3(\rho_1-\rho_2)}{\epsilon_0\hbar^2}\mu_{12}^2\delta_{12}\times\frac{\omega_{12}^2\left[1+\frac{\Gamma_2}{\Gamma_1}\right]+(\omega^2+\Gamma_2^2)\left[\frac{\Gamma_2}{\Gamma_1}-1\right]}{[(\omega_{12}-\omega)^2+\Gamma_2^2][(\omega_{12}+\omega)^2+\Gamma_2^2]} \ . \tag{26}$$

It is clear that optical rectification will occur in asymmetric QW's where the centroids of the electrons in states $|\zeta_1\rangle$ and $|\zeta_2\rangle$ are different ($\delta_{12}\neq0$). The OR coefficient at a desired frequency ω will be maximum if the QW is designed so that the energy difference E_2-E_1 corresponds to a resonance condition, i.e., $\omega\approx\omega_{12}$ ($\Gamma_1\ll\Gamma_2\ll\omega_{12}$):

$$\chi_{0,\max}^{(2)}=2\frac{q^3T_1T_2}{\epsilon_0\hbar^2}(\rho_1-\rho_2)\mu_{12}^2\delta_{12} \ . \tag{27}$$

The electro-optic coefficient r of an AQW may be obtained from $\chi_0^{(2)}$ by $r=\chi_0^{(2)}/\epsilon_R^2$,[24] where ϵ_R is the relative permittivity of the AQW at the frequency ω. In order to compare the electro-optic coefficients obtained in AMQW's and in other materials, we must normalize Eq. (27) to a volume. The normalization procedure, which tends to limit the total size of the AMQW's in order to enhance the linear density of QW's, plays a similar role in the optimization of hyperpolarizable molecules for optical nonlinearities. For the clarity of the physics, we shall make the assumption in the following that the thickness of the $Al_xGa_{1-x}As$ potential barrier is thin enough so that the filling factor is taken equal to 1. Equation (27) may then be rewritten to give the volume electro-optic coefficient

$$r_{\max}=2\frac{q^3T_1T_2}{\epsilon_R^2\epsilon_0\hbar^2}(\rho_1-\rho_2)\frac{\mu_{12}^2\delta_{12}}{L} \ , \tag{27'}$$

where L is the width of the quantum well. Let us note that, by taking the volume density of carriers in the ith subband as ρ_i/L, one neglects the spatial variations of carrier density due to space-charge effects.

B. Second-harmonic generation in a three-level system

The density matrix associated with SHG is obtained by inserting Eq. (23) in Eq. (18), which yields

$$[\tilde{\rho}_{2\omega}^{(2)}]_{ij}=\frac{1}{\hbar(2\omega+\omega_{ji}-i\Gamma_{ji})}[qz,\tilde{\rho}^{(1)}]_{ij}\tilde{E} \ . \tag{28}$$

Using Eq. (22) for $\rho^{(1)}$ and Eq. (19) for the definition of $\chi_{2\omega}^{(2)}$, we find easily

$$\chi_{2\omega}^{(2)}=\frac{q^3}{\epsilon_0\hbar^2}\sum_i\sum_k\frac{1}{(2\omega+\omega_{ik})-i\Gamma_{ki}}\sum_l\mu_{ik}\mu_{kl}\mu_{li}\left[\frac{\rho_i-\rho_l}{(\omega+\omega_{il})-i\Gamma_{li}}-\frac{\rho_l-\rho_k}{(\omega+\omega_{lk})-i\Gamma_{kl}}\right] \ . \tag{29}$$

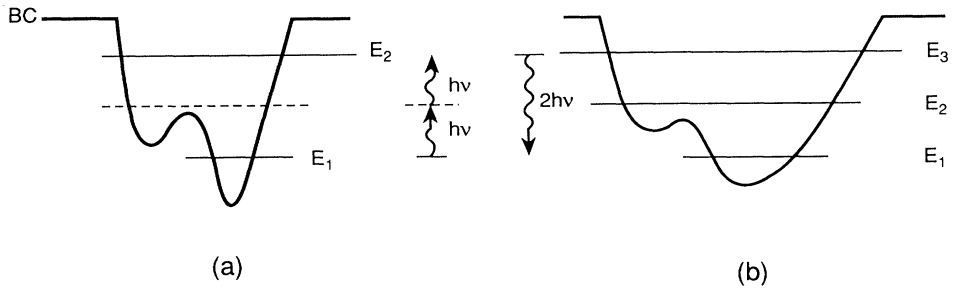

FIG. 1. Energy-band diagram of asymmetric quantum wells with (a) a virtual and (b) a real intermediate state, leading to single- and double-resonance conditions, respectively. Optical transitions are symbolized by arrows.

This sum has a sharp maximum if the condition of double resonance can be met (see Fig. 1), i.e., $\omega \approx \omega_{12} \approx \omega_{23} \approx \Omega$:

$$\chi^{(2)}_{2\omega} = \frac{q^3(\rho_1 - \rho_2)}{\epsilon_0 \hbar^2} \frac{\mu_{12}\mu_{23}\mu_{31}}{(\omega - \Omega - i\Gamma_2)(2\omega - 2\Omega - i\Gamma_2)} . \quad (30)$$

Once again, it is clear that the product $\mu_{12}\mu_{23}\mu_{31}$ is identically zero for symmetric wave functions. The volume SHG coefficient has a peak value for $\omega \approx \Omega$ given by

$$\chi^{(2)}_{2\omega,\max} = \frac{q^3(\rho_1 - \rho_2)}{\epsilon_0} \frac{\mu_{12}\mu_{23}\mu_{31}}{L} \frac{1}{(\hbar\Gamma_2)^2} . \quad (31)$$

At this stage, it is interesting to compare the enhancement of the SHG coefficient due to the double-resonance effect to the one calculated by Tsang, Ahn, and Chuang[25] in a single-resonance QW biased by an electric field. Direct application of Eq. (29) for $2\omega \approx \omega_{12}$ leads to

$$\xi^{(2)}_{2\omega} = \frac{q^3(\rho_1 - \rho_2)}{\epsilon_0 \hbar^2} \frac{\mu_{12}^2 \delta_{12}}{(\omega - \omega_{12} - i\Gamma_2)(2\omega - \omega_{12} - i\Gamma_2)} . \quad (32)$$

One may then take the ratio between the maximum SHG coefficients:

$$\left| \frac{\chi^{(2)}_{2\omega,\max}}{\xi^{(2)}_{2\omega,\max}} \right| = \frac{|\mu_{12}\mu_{23}\mu_{31}|}{|\mu_{12}^2 \delta_{12}|} \frac{\omega_{12}}{2\Gamma_2} . \quad (33)$$

Apart from the geometrical factor $|\mu_{12}\mu_{23}\mu_{31}/\mu_{12}^2\delta_{12}|$, the main gain in the double-resonance structure is thus due to the long lifetime T_2 of the electrons in the intermediate level E_2 compared to the lifetime ω_{12}^{-1} in the virtual level in the single-resonance structure.

Another important point is the breakdown of Miller's empirical rule.[24] Indeed, because of the double-resonance effect in these quantized structures, it is straightforward to show that the Miller coefficient is proportional to the photon energy and thus cannot be a universal constant.

IV. QUANTUM LIMITATION TO SECOND-ORDER SUSCEPTIBILITIES

From Eqs. (27) and (31), it is clear that, in order to maximize the second-order susceptibilities e.g., the OR coefficient, there is a tradeoff to be made between μ_{12} and δ_{12}. An increase of the QW asymmetry will decrease the overlap integral in μ_{12} but enhance the mean electron displacement δ_{12}. This tradeoff should lead to a quantum limitation of geometrical origin in the second-order susceptibilities. For this purpose, we thus need a QW potential model where one can tune as independently as possible the quantized energies E_i, the total thickness, and the asymmetry.

The simplest model we can think of is an infinitely deep potential well of total thickness L, divided in two parts (see Fig. 2),

$$V(z) = \begin{cases} 0 & \text{for } 0 < z < d \\ V & \text{for } d < z < L \end{cases} . \quad (34)$$

A somewhat similar model has been proposed by Goossen and Lyon[26] to study the dielectric function of an asymmetric QW with $L \to \infty$ and by Yuh and Wang[9] to study Stark shifts in such structures. Our purpose, however, is different from theirs. For each photon energy $h\nu$, we are going to tune the three parameters (d, V, L) to optimize the OR and the SHG coefficients, respectively; that is, considering the results of the preceding section, to

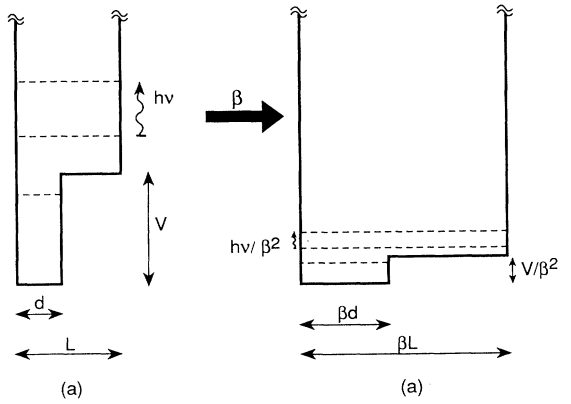

FIG. 2. Scaling rules for infinite-step asymmetric quantum wells.

meet the following conditions.

Condition 1,

$$E_2-E_1=h\nu \text{ for the OR case ;}$$

Condition 2,

$$E_3-E_2=E_2-E_1=h\nu \text{ for the SHG case .}$$

Before describing our optimization procedure, we are going to derive an important scaling rule, which will allow us to obtain the variation of the maximum second-order susceptibilities as a function of the photon energy.

A. Photon energy scaling rule for maximum second-order susceptibilities

Let us assume that the optimization problem for the OR coefficient has been solved for a photon energy $h\nu$, that is, we have found the triplet (d,L,V) which maximizes the $\mu_{12}^2\delta_{12}$ product calculated from the wave functions $\zeta_i(z)$, solution of the Schrödinger equation:

$$-\frac{\hbar^2}{2m^*}\frac{d^2}{dz^2}\zeta_i(z)+[V(z)-E]\zeta_i(z)=0 \tag{35}$$

with $E_2-E_1=h\nu$. Let us introduce the variable $u=\alpha z$ in Eq. (35), where α is a length scaling factor. It is clear that the wave function $\zeta_i^\alpha(u)=(1/\sqrt{\alpha})\zeta_i(u/\alpha)$ is solution of the Schrödinger equation with potential profile $V^\alpha(u)=(1/\alpha^2)V(u/\alpha)$, which is shown in Fig. 2. The eigenenergies satisfy $E^\alpha{}_2-E^\alpha{}_1=(E_2-E_1)/\alpha^2$ and the corresponding product of dipolar matrix elements $\mu^\alpha{}_{12}{}^2\delta^\alpha{}_{12}$ is maximized for $d^\alpha=\alpha d$ and $L^\alpha=\alpha L$ and thus

$$\mu^\alpha{}_{12}{}^2\delta^\alpha{}_{12}=\alpha^3\mu_{12}{}^2\delta_{12} . \tag{36}$$

Considering the scaling rules for $\mu^\alpha{}_{12}{}^2\delta^\alpha{}_{12}$, $E^\alpha{}_2-E^\alpha{}_1$ and the triplet $(V^\alpha,d^\alpha,L^\alpha)$, one may thus formulate the following laws.

For each photon energy $h\nu$, the optimized potential profile (d,L,V) for a given nonlinear susceptibility is given by

$$\begin{aligned} d&=C_1 d_\nu , \\ L&=C_2 d_\nu , \\ V&=C_3 h\nu , \end{aligned} \tag{37}$$

where d_ν is given by

$$d_\nu=\frac{\hbar\pi}{\sqrt{2m^*h\nu}} , \tag{38}$$

d_ν is the width of a QW for which the confinement energy E_1 is equal to the desired photon energy $h\nu$, e.g., $d_\nu=6.9$ nm for a 10.6-μm photon. We are thus left with the problem of finding the triplet (C_1,C_2,C_3), i.e., the "best potential shape," for each type of nonlinear susceptibility optimization. We will show below that C_1,C_2 are in the 0.1–1 range so that d_ν is indeed the length scale which is relevant to our problem.

Given Eqs. (27) and (31) and including the scaling laws, the values of the maximum volume second-order nonlinear susceptibilities are thus given, respectively, by

$$r_{\max}(h\nu)=g_{\rm OR}\pi^2\frac{q^3}{\epsilon_0}\frac{T_1T_2}{m^*\epsilon_R^2}\rho_S\frac{1}{h\nu} \tag{39}$$

and

$$\chi^{(2)}_{2\omega,\max}(h\nu)=g_{\rm SHG}\frac{\pi^2}{2}\frac{q^3}{\epsilon_0}\frac{T_2^2}{m^*}\rho_S\frac{1}{h\nu} . \tag{40}$$

$g_{\rm OR}$ and $g_{\rm SHG}$ are dimensionless quantities corresponding to the ratios $\mu_{12}{}^2\delta_{12}/Ld_\nu^2$ and $\mu_{12}\mu_{23}\mu_{31}/Ld_\nu^2$, respectively, which may be obtained from the triplet (C_1,C_2,C_3).

These limitations to second-order susceptibilities in quantum structures are very different in nature from the preceding ones, the most famous being the classical "polarizable sphere" model of Gurnick and DeTemple, which yields an $(h\nu)^{-2}$ dependence of $r_{\max}$ and $\chi^{(2)}_{2\omega}$.[5]

B. Maximization of the electro-optic coefficient in a step QW

The optimization scheme is the following. For an arbitrary photon energy, e.g., 50 meV, one varies d and V, calculates L so that Condition 1 is met, solves the Schrödinger equation, and computes the $\mu_{12}{}^2\delta_{12}$ product. Figure 3 shows the variation of $\mu_{12}{}^2\delta_{12}/d_\nu^2L$ as a function of L for different values of d ranging from 1 to 17 nm. It is clear from this figure that the maximum value is obtained for $d\to 0$ and $V\to\infty$. It can be shown (see the Appendix) that the optimum triplet is

$$\begin{aligned} &L/d_\nu=\theta/\pi , \\ &V=\frac{\pi^2\hbar^2}{8m^*d^2}\to\infty, \quad \text{as } d\to 0 , \end{aligned} \tag{41}$$

where θ is solution of $\tan\theta=\theta$, i.e., $\theta=4.49$. Moreover, the dimensionless coefficient $g_{\rm OR}$ is given by

$$g_{\rm OR}=\frac{3}{2\pi^2}\frac{(1-\cos\theta)^4}{\theta^4\cos^2\theta}\approx 1.733\times 10^{-2} . \tag{42}$$

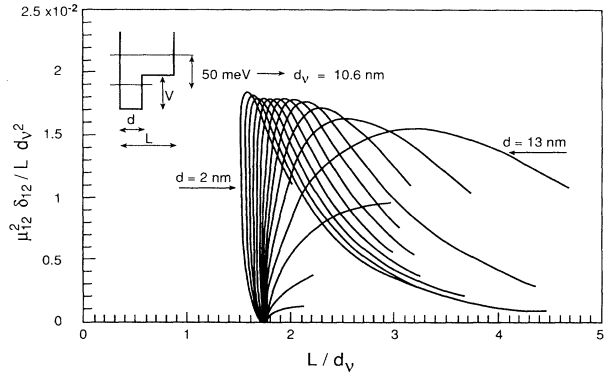

FIG. 3. Variation of the product of normalized dipolar matrix elements $\mu_{12}{}^2\delta_{12}/Ld_\nu^2$ as a function of the total AQW thickness L/d_ν for different values of the deep QW thickness d. The energy difference E_2-E_1 is kept equal to 50 meV. These curves show that the maximum value of the electro-optical coefficient r is obtained for $d\to 0$, i.e., for a diverging asymmetry.

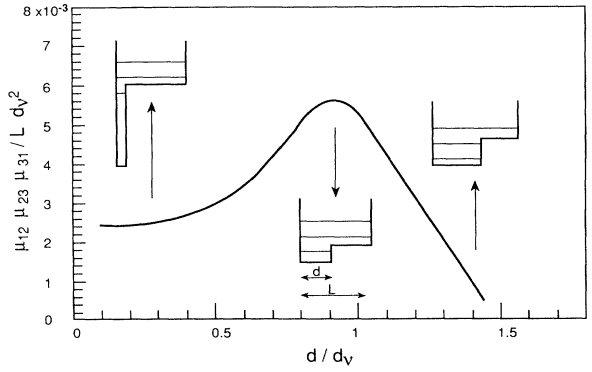

FIG. 4. Variation of the product of the normalized dipolar matrix elements $|\mu_{12}\mu_{23}\mu_{31}|/Ld_\nu^2$ as a function of deep QW thickness d. The double-resonance conditions $E_2-E_1=E_3-E_2=h\nu$ are imposed in the calculation. The optimum value $d/d_\nu=0.925$ defines the "best potential shape" for second-harmonic generation in step AQW's.

For practical purposes, the convergence is extremely fast so that a triplet such as $(d/d_\nu=0.2, L/d_\nu=1.6, V/h\nu=8.6)$ is already an excellent estimation of the "best potential shape" for optical rectification or electro-optic coefficients.

C. Maximization of the second-harmonic coefficient in a step QW

Condition 2 imposes two relations between d, L, and V so that only one parameter may be varied for the optimization procedure. Figure 4 shows the variation of $|\mu_{12}\mu_{23}\mu_{13}|/d_\nu^2 L$ with d/d_ν. The maximum value is obtained for $d/d_\nu=0.925$ for which $L/d_\nu=2.14$, $V/h\nu=1.08$, and $g_{\mathrm{SHG}}=5.68\times10^{-3}$. Let us recall once again that these optimized geometrical factors hold for every photon energy.

Table I summarizes the different values resulting from this optimization procedure. Figures 5(a) and 5(b) show

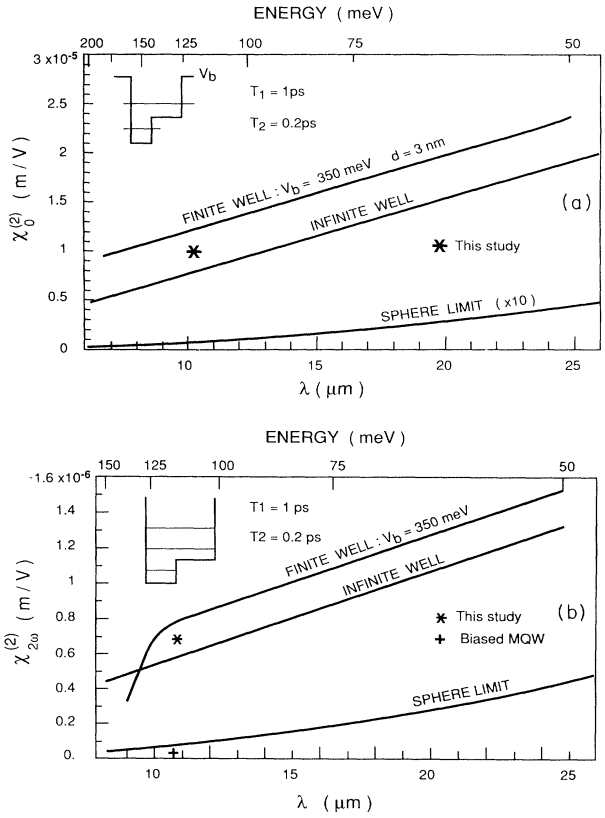

FIG. 5. Quantum limitation of (a) optical rectification and (b) second-harmonic in step AQW's. The diagonal and off-diagonal relaxation times are 0.2 and 1 ps, respectively. The results are compared with the "polarizable sphere limit" of Gurnick and DeTemple (Ref. 5).

the maximum second-order nonlinear susceptibilities (optical rectification and second harmonic generation, respectively) as a function of photon energy obtained in this model. We have assumed usual relaxation times of $T_2=0.2$ ps and $T_1=1$ ps.[11] These curves are compared with the one given by the classical "polarizable sphere"

TABLE I. Values of the three parameters d, L, and V characterizing asymmetric step quantum wells and optimizing, respectively, the quantum numbers μ_{12}^2/Ld_ν^2 and $\mu_{12}\mu_{23}\mu_{31}/Ld_\nu^2$, i.e., the optical rectification and second-harmonic-generation coefficients, respectively. The results are given for an infinitely deep quantum well ($\Delta E=\infty$) and an $Al_{0.4}Ga_{0.6}As/GaAs$ one ($\Delta E=350$ meV).

		Optical rectification		Second-harmonic generation	
		$\Delta E=\infty$	$\Delta E=350$ meV	$\Delta E=\infty$	$\Delta E=350$ meV
Remarks	Limit	Approximation $h\nu=100$ meV $d_\nu=74.9$ Å	$h\nu=100$ meV $d_\nu=74.9$ Å		$h\nu=100$ meV $d_\nu=74.9$ A
d/d_ν	0	0.19	0.40	0.92	0.68
L/d_ν	1.43	1.59	1.37	2.14	1.68
$V/h\nu$	∞	8.60	1.40	1.08	1.12
$\frac{\mu_{12}^2\delta_{12}}{Ld_\nu^2}$	1.74×10^{-2}	1.85×10^{-2}	2.51×10^{-2}		
$\frac{\mu_{12}\mu_{23}\mu_{31}}{Ld_\nu^2}$				5.67×10^{-3}	7.48×10^{-3}

limit of Gurnick and deTemple.[5] In their paper, these authors estimate that the classical model leads to limit values which are higher than the ones obtained using the quantum Morse potential model. This is not so in our case. The huge enhancement in the theoretical values of the maximum susceptibilities in our model comes from (i) a larger asymmetry and (ii) the possibility of independently tuning the asymmetry and the resonance conditions in step QW's compared to a Morse potential. Let us note finally that an infinite potential well, such as used in this theoretical part, is of course not physically feasible. For instance, the maximum barrier height one may obtain in the $GaAs/Al_xGa_{1-x}As$ system is 350 meV for $x=40\%$. Above this Al concentration, the Γ and X valleys cross and the effective barrier decreases. No simple theoretical results may then be inferred. Nevertheless, the exact numerical simulations show that the infinite potential well is a good approximation of the physical case and that scaling laws are still particularly well satisfied [see Table I and Figs. 5(a) and 5(b)]. It should be noted that the values obtained in finite QW's are higher than in infinite ones. This is due to the contribution of the evanescent part of the electron wave functions.

V. EXPERIMENTAL REALIZATIONS

A. Optical rectification in AMQW's

In order to test our model, samples have been grown by molecular-beam epitaxy. The samples used for optical rectification consist of 12 periods of (3 nm GaAs)–(6.5 nm $Al_{0.2}Ga_{0.8}As$) wells separated by 50-nm-thick $Al_{0.4}Ga_{0.6}As$ barriers epitaxially grown on a 3×10^{18} cm^{-3} Si-doped GaAs substrate. The ratios d/d_v, L/d_v, and $V/h\nu$, are 0.43, 1.4, and 1.37, respectively, for a photon energy of 118 meV. These values are very similar to the optimized ones, as indicated in Table I. Figure 6 indicates the band diagram and the square of the envelope wave functions of the resulting AQW structure. From this calculation, we find $\mu_{12}=1.76$ nm and $\delta_{12}=3.96$ nm. The $Al_xGa_{1-x}As$ barrier thickness has been chosen rather large and the Al composition sufficiently high so that the structure is completely insulating at liquid-nitrogen temperature. The GaAs well is uniformly doped at 0.5 nm from the interfaces, in order to yield a carrier concentration of 10^{11} cm^{-2}, while the rest of the wells and barriers are nonintentionally doped. The whole structure is clad between two 300-nm thick Si-doped (10^{18} cm^{-3}) GaAs contacting layers. Mesa n^+-i-n^+ structures (600×500 μm^2) are fabricated, using a standard photolithography technique and AuGeNi alloy contacts are taken on the rear and top surfaces. Annular contacts are used in order to allow front illumination.

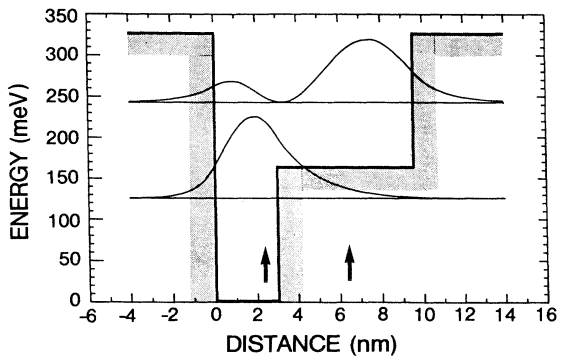

FIG. 6. Energy-band diagram and square of the wave functions of the step AQW used in the optical rectification study.

Because of the high density of carriers in the Ohmic contacts and in the GaAs wafer, Hall measurements and absorption spectra cannot be performed in such a structure. Consequently, a similar sample has been grown on a semi-insulating GaAs wafer, with 50 periods of the same characteristics as the preceding structure but without the GaAs contacting layers. Hall measurements indicate a carrier concentration of 1.1×10^{11} cm^{-2} with a mobility of 4200 cm^2/V s at 4 K. Absorption spectroscopy is realized in a Fourier-transform infrared spectrometer at 4 K. The absorption exhibits a Lorentzian line shape with a peak at 10.0 μm with a value of 2.0×10^{-4} per well at Brewster angle. Using Eq. (7), we find a dephasing time T_2 of 0.19 ps.

The principle of measurements of the optical rectification coefficient is the following. For an electromagnetic field propagating in the direction parallel to the QW's, the dipoles which build up in the AMQW's induce, if the material is insulating, a polarization $P=\epsilon_0\chi_0^{(2)}E^2$. A steady-state electric field $P/\epsilon_0\epsilon_{stat}$ appears in each QW (Ref. 27) yielding a voltage V at the diode terminals given by

$$V=NL\frac{\chi_0^{(2)}\eta_0 P_W}{\epsilon_{stat}}, \tag{43}$$

where P_W is the incident beam power, η_0 is the vacuum impedance (377 Ω), N is the number of AQW's, and ϵ_{stat} is the effective static dielectric constant that we take equal to 13. This bias is measured using a lock-in technique, while the sample is illuminated by a continuous CO_2 laser chopped by a mechanical chopper (500–3000 Hz).

The sample is mounted in a liquid-N_2 cryostat equipped with ZnSe windows. In order to study the influence of the angle of incidence, θ, of the optical beam relative to the sample surface, the cryostat is mounted on a goniometer. Two configurations may be used: S (TE), where the polarization vector is perpendicular to the plane of incidence, i.e., parallel to the surface of the sample, and P (TM), where the polarization vector is in the plane of incidence. Moreover, the polarization and the intensity of the optical beam may be varied using a grating polarizer and a half-wave plate. Figure 7 shows the induced voltage (laser power 60 W/cm^2) as a function of the angle of incidence for the P polarization configuration. The bars indicate the experimental uncertainties. The signal presents a well-defined maximum near the Brewster angle. This is due to the combined effect of (i) the angular dependence of the coupling of the electromagnetic field with the quantized electron gas and

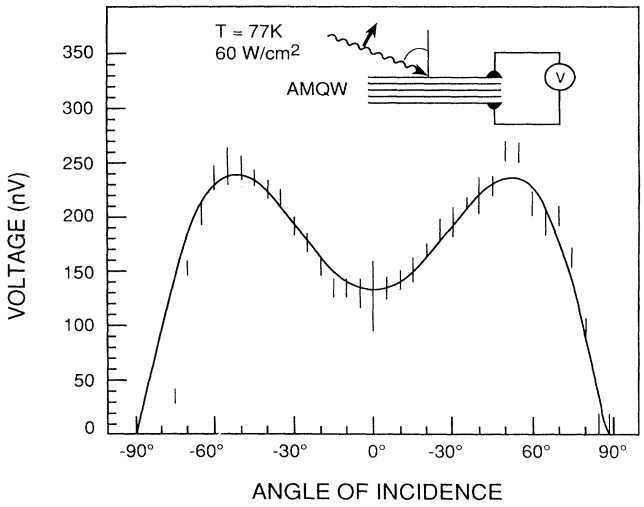

FIG. 7. Optical rectification signal appearing in the 12-period MQW's described in Fig. 6 as a function of the angle of incidence. The sample is illuminated by a CO_2 10.6-μm laser with a power of 60 W/cm^2 in the P (TM) polarization.

(ii) the variation of the power transmitted into the sample, which drops off rapidly from Brewster angle to grazing incidence. Taking both effects into account, the optical rectification voltage $V(\theta)$ which appears at the diode terminals is

$$V(\theta)=8\frac{\cos^2\theta\sin^2\theta}{\epsilon_R\cos\theta+\sqrt{\epsilon_R-\sin^2\theta}}V\ . \tag{44}$$

We have represented in Fig. 7 the best fit between our experimental data and a combination of a thermal effect (which yields the nonzero voltage at $\theta=0°$) and the optical rectification using Eqs. (43) and (44). The agreement is quite good and we deduce an OR coefficient of 5.25×10^{-6} m/V in the wells, indicated in Fig. 5(a) for comparison purposes. Using Eq. (27) with the calculated value of μ_{12} and δ_{12}, we deduce a diagonal relaxation time T_1 of 0.6 ps, which is smaller than what is usually quoted in the literature. The corresponding effective electro-optic coefficient r is thus 7.2 nm/V (correcting for the filling factor of only 15%), which is more than three orders of magnitude higher than in bulk GaAs.

An examination of Eq. (27) shows different ways to enhance the OR coefficient: the geometrical factor $\mu_{12}{}^2\delta_{12}$, which has already been addressed in Sec. IV, the doping concentration ρ_s, which is limited by the solubility limit of Si in GaAs ($\approx2\times10^{18}$ cm^{-3}), and the time constant product T_1T_2. T_2 is certainly governed by intrinsic mechanisms such as electron-electron interaction or optical-phonon emission for an excitation energy higher than 36 meV,[28] without clear possibilities to act upon it. On the other hand, T_1 is a population relaxation time and can be enhanced by storing the excited electrons on a metastable level $|\zeta_3\rangle$, which interacts slowly with the ground state $|\zeta_1\rangle$. Such a device is schematically represented in Fig. 8. It consists of two GaAs quantum wells (QW1 and QW2), separated by an intermediate

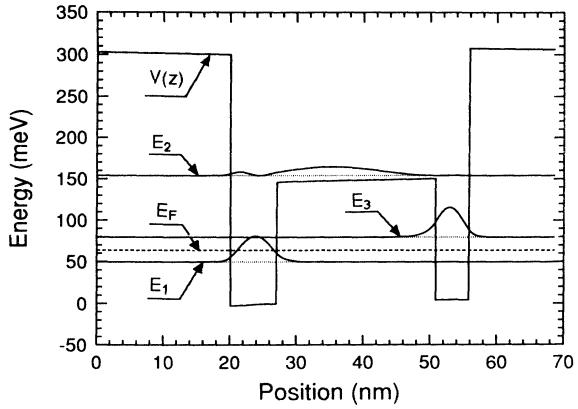

FIG. 8. Energy-band diagram and square of the wave functions of the double AQW used in the optical rectification study.

$Al_xGa_{1-x}As$ barrier, clad between two $Al_yGa_{1-y}As$ barriers, with $y>x$. Under illumination, the electrons are excited from level $|\zeta_1\rangle$ to $|\zeta_2\rangle$, which is delocalized between both wells. Part of the electrons will recombine on level $|\zeta_3\rangle$, where they will be stored until they are transferred back into QW1 by thermal emission or tunneling (depending on temperature) with a characteristic time τ. The asymmetry of the structure is due to the difference of widths between QW1 and QW2. The structure must moreover fulfill the following conditions: the energy difference E_2-E_1 must be close to the photon energy $h\nu$, the energy difference E_3-E_1 must be large compared to kT (6.56 meV at 77 K), and the intermediate barrier must be thick enough to induce a large transfer time between QW1 and QW2.

A complete calculation of the OR coefficient in this three-level system is feasible using the results of Sec. III but extremely tedious. The philosophy of the calculation is that the double resonance $|\zeta_1\rangle\rightarrow|\zeta_2\rangle\rightarrow|\zeta_1\rangle$ in the two-level structure will be replaced by the resonance $|\zeta_1\rangle\rightarrow|\zeta_2\rangle\rightarrow|\zeta_3\rangle$ in the three-level one. Consequently, the product $\mu_{12}{}^2\delta_{12}$ will be replaced by $\mu_{12}\mu_{23}\delta_{13}$ and the product T_1T_2 by the product τT_2. The dipole P' of this structure may thus be compared to the preceding one P[12]:

$$\frac{P'}{P}\approx\frac{\mu_{13}\delta_{13}}{2\mu_{12}\delta_{12}}\frac{\tau}{T_1}\ . \tag{45}$$

Most of the gain in this structure will come from the enhancement of the ratio τ/T_1, the geometrical factor $\mu_{ij}\delta_{ij}$ being bounded by quantum limits as stated in Sec. IV. In the case of the structure in Fig. 8, using a diffusion model based on a Frohlich interaction, the tunneling time is estimated at 10 ps, i.e., a gain of 20 compared to the structure of Fig. 6.[29]

The structure corresponding to Fig. 8 has been grown by MBE. It consists of 50 periods of QW's (QW1: 7 nm of GaAs; intermediate barrier: 24 nm of $Al_{0.18}Ga_{0.82}As$; QW2: 5 nm of GaAs) separated by 34-nm-thick $Al_{0.36}Ga_{0.64}As$ barriers, epitaxially grown on a 3×10^{18}

cm^{-3} Si-doped GaAs substrate. QW1 is 4.3×10^{11} cm^{-2} Si doped while the rest of the wells and barriers are nonintentionally doped. The structure is clad between two contacting layers and processed like the preceding one. Figure 9 shows the induced voltage as a function of angle of incidence θ for polarizations S and P at a laser power of 6.3 W/cm^2 for a sample temperature of 77 K. The sharp peak at the Brewster angle is observed in the P polarization but absent in the S one where no coupling can exist between the electromagnetic waves and the quantized electron gas. Note that the signal values of the rectification signal at zero angle are both equal in both configurations, confirming the thermal nature of the signal at $\theta=0°$. The value of the OR coefficient is 1.62×10^{-3} m/V in each well, which is 310 times higher than in the single-QW structure. We attribute this enhancement factor to a gain of 4 on the carrier concentration, a factor of 2.5 on the $\mu_{ij}\delta_{ij}$ product, according to dipole matrix element calculations, and a factor of 30 for τ compared to T_1, i.e., 18 ps instead of 0.6 ps. Finally, the optically resonant character of the OR signal is confirmed by studying the spectral response of this AMQW's, using a tunable grating CO_2 laser. The resulting curve, shown in Fig. 10, has been obtained at 77 K, for a laser power of 30 mW, at a Brewster angle in the P polarization configuration. The noise is largely due to the geometrical fluctuations of the beam when varying the wavelength. The spectral response is Lorentzian, peaked around 11 μm with a somewhat large half-maximum linewidth [full width at half maximum (FWHM)] of 20 meV. We attribute this large width to the contribution of additional quantized levels in this rather large quantum well.

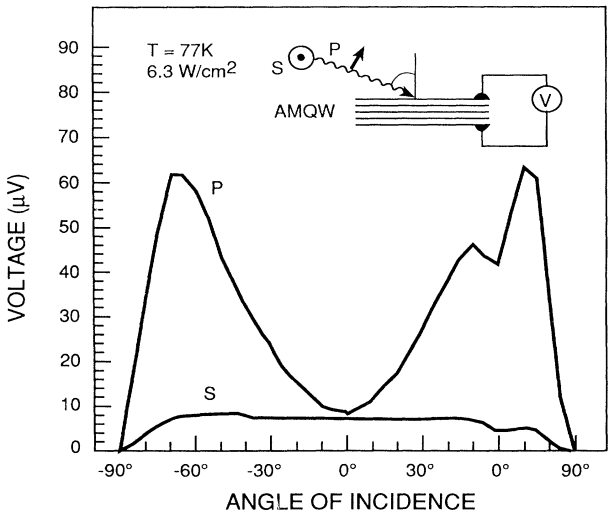

FIG. 9. Optical rectification signal appearing in the 50-period MQW's described in Fig. 8 as a function of the angle of incidence. The sample is illuminated by a 10.6-μm CO_2 laser with a power of 6.3 W/cm^2 in both polarizations. The signal at 0° is the residual thermal signal.

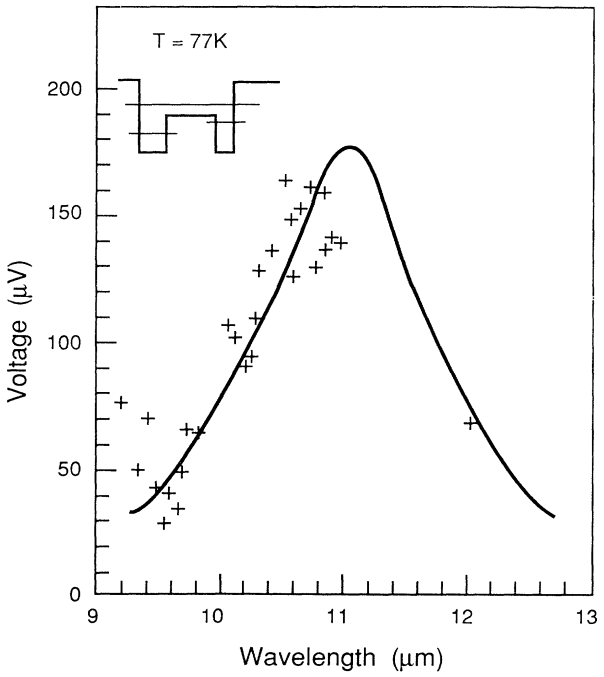

FIG. 10. Wavelength dependence of the optical rectification signal in the double AQW of Fig. 8. The sample is illuminated by a tunable grating CO_2 laser.

B. Second-harmonic generation in AMQW's

Samples used in our experiments have been chosen as close as possible to the ideal structures described in Sec. IV. The structures grown by MBE consist of 100 periods of (6 nm GaAs)–(4.5 nm $Al_{0.1}Ga_{0.9}As$) wells separated by 30 nm $Al_{0.4}Ga_{0.6}As$ barriers epitaxially grown on a semi-insulating GaAs wafer. The calculated resulting band diagram of this AQW is shown in Fig. 11. The dipole matrix elements given by the numerical resolution of the Schrödinger equation are $\mu_{12}=2.1$ nm, $\mu_{23}=3.0$ nm, and $\mu_{13}=0.38$ nm. The GaAs wells are doped in their centers

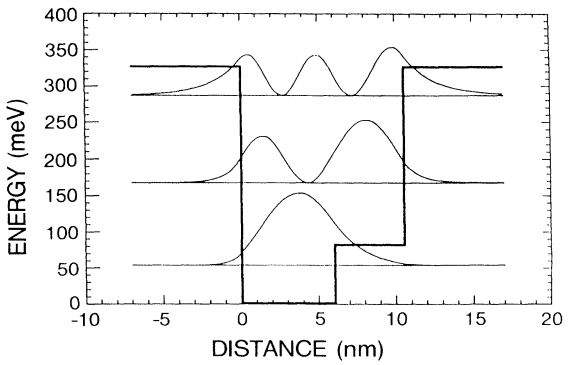

FIG. 11. Energy-band diagram and square of the wave functions of the step AQW used in the second-harmonic-generation study.

providing a 2.2×10^{11} cm^{-2} donor concentration as checked by Hall measurement, whereas the rest of the sample is nonintentionally doped. The absorption spectrum at room temperature, shown in Fig. 13, exhibits a peak at 11.3 μm with a value of 3.3×10^{-4} per well at the Brewster angle. Given the value of μ_{12} and ρ_s, using Eq. (7) for the absorption, we find a dephasing time T_2 of 0.14 ps, which is in good agreement with the results obtained in the OR samples. Let us note that the transition $E_1\rightarrow E_3$ is not visible in our infrared spectrum. This is due to the small value of μ_{13} compared to μ_{12}. This result differs from the result of Mii *et al.* who used a special QW design in which $E_1\rightarrow E_2$ and $E_1\rightarrow E_3$ transitions have similar oscillator strengths.[30]

The measurements are made using the same laser sources as in the preceding OR experiments. Care is taken to eliminate the undesirable luminescence lines of the laser source (mostly 5.3 μm) by means of an InSb or interferometric filter. The SHG signal is detected in a cooled InSb or a room-temperature pyroelectric detector. The 10-μm laser beam is prevented from illuminating the detectors by means of a sapphire window. Experiments are done at room temperature. Figure 12 shows the SHG signal as a function of the angle of incidence for a P polarization in an AMQW structure and in the bulk GaAs substrate. The signal is almost absent in the latter case, though the total thickness of the GaAs wafer is 300 μm while it is only 10 μm in the AMQW's. *Note also that the SHG is so intense that no phase matching is necessary.* At the Brewster angle where all the power is transmitted to the crystal, the SHG yield $P_{2\omega}/P_\omega$ is then given by[24]

$$\frac{P_{2\omega}}{P_\omega}=2\eta_0^3\epsilon_0^2\frac{\omega^2(|\chi^{(2)}_{2\omega}|NL)^2}{\epsilon_R^3}P_\omega\ . \tag{46}$$

Figure 12 indicates a yield of 1.0×10^{-7} for 1 W of pump power, that is, an experimental value of the SHG coefficient of 7.2×10^{-7} m/V. This value is 1900 times greater than the one found in bulk GaAs, which is already a good nonlinear material in the infrared, and about 26 times greater than the value obtained by Fejer *et al.* in biased quantum wells.[8] Once again, this enhancement of the SHG coefficient in our structure is due to the doubly resonant nature of the optical transitions in our AQW's compared with biased symmetric ones.

Figure 13 shows the second-harmonic power as a function of the pump laser wavelength. This spectral response is fitted by the product of the Lorentzian line shapes given by Eq. (30) using the value of Γ_2 obtained from absorption experiments. The agreement between experiment and theory is excellent. The apparent decrease in the FWHM linewidth in the SHG spectrum compared to that of the absorption one is in excellent agreement with theoretical predictions. Indeed, if we calculate the ratio between the FWHM of the Lorentzian line shape $1/[(\omega-\omega_{12})^2+\Gamma^2]$ and the product of the Lorentzian line shapes found in Eq. (30), i.e, $1/[(2\omega-2\omega_{12})^2+\Gamma^2][(2\omega-2\omega_{12})^2+\Gamma^2]$, we find a value of 2.38 while an experimental ratio of 2.5 is obtained. This decrease in the linewidth is a consequence of the coherent origin of the second-harmonic-generation mechanism. Let us note finally the small shift in the peak position between the absorption and the SHG spectral curves. We attribute this fit to a small difference between energies E_3-E_2 and E_2-E_1.

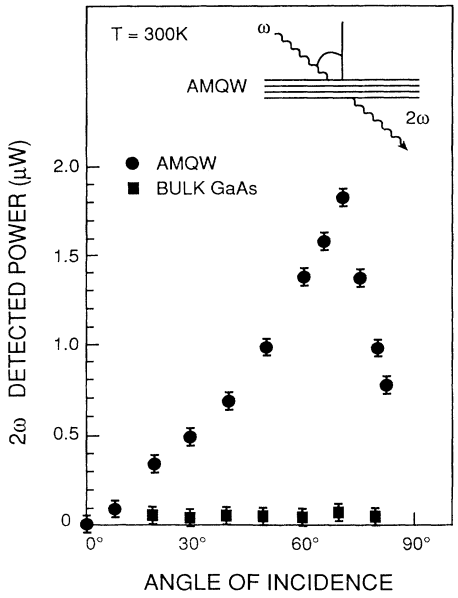

FIG. 12. Second-harmonic power detected at 5.3 μm in the 100-period AQW's excited at 10.6 μm. The laser power is approximately 10^4 W/cm^2. The second-harmonic power detected in the GaAs substrate after chemical etching is shown for purposes of comparison.

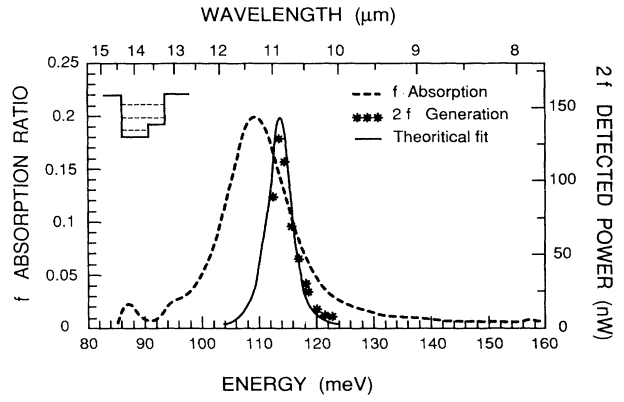

FIG. 13. Variation of the second-harmonic-generation yield as a function of the grating CO_2 laser excitation wavelength and transmission spectrum obtained by Fourier-transform infrared spectroscopy of AQW's. Experimental points are taken from Ref. 14.

VI. CONCLUSION

In this paper, we have presented a concise formulation of second-order optical nonlinearities in asymmetric quantum wells. The origin of the large oscillator strengths in GaAs QW's is analyzed in terms of the contribution of the optical transitions over the whole band structure of GaAs. The normalized dipolar matrix elements $\mu_{12}\mu_{23}\mu_{31}/L$ or $\mu_{12}^2\delta_{12}/L$ (L is the total QW thickness) which lead to the maximum values of the second-order susceptibilities are expressed in terms of the product gd_ν^2: g is a universal geometrical factor while d_ν is the width of the QW in which the energy of the first quantized level E_1 is equal to the photon energy $h\nu$. This simplified approach allows us to introduce additional quantum limitations to second-order optical nonlinearities in asymmetric quantum wells with the different relaxation times left as parameters. We thus show that the huge nonlinearities observed in these structures are due to (i) the effect of the small effective mass (which was already addressed in the literature), but mainly from (ii) the double-resonance effect that can be designed in these AQW's. Values of optical rectification coefficients as high as 1.6×10^{-3} m/V at 10.6 μm (i.e., six orders of magnitude higher than in bulk GaAs) may be obtained in optimized structures while a second-harmonic-generation coefficient of 7.2×10^{-7} m/V at 10.6 μm is found in AQW's that is more than three orders of magnitude higher than in bulk GaAs. All these experimental results are in excellent agreement with our simplified theoretical approach and show that these AQW's really behave as giant "pseudomolecules" optimized for optical nonlinearities in the infrared.

ACKNOWLEDGMENTS

This work would have not been possible without the help of many fruitful discussion with various colleagues. Among them, we are particularly indebted to Dr. B. Vinter and Professor C. Weisbuch from Thomson-CSF, Dr. J. Zyss, Dr. I. Abram, and Dr. J. L. Oudar from the Centre National d'Etudes des Télécommunications (Bagneux), Professor C. Flytzanis, Dr. G. Lampel, and Professor C. Hermann from the Ecole Polytechnique (Paris), and Professor G. Fishman from the CNRS (Grenoble). We would like to thank the team of the Institut d'Electronique Fondamentale in Orsay (Dr. J. M. Lourtioz and Dr. F. Julien) for their collaboration in the experimental work of second-harmonic generation in asymmetric quantum wells.

APPENDIX: SOLUTION OF THE SCHRÖDINGER EQUATION FOR AN INFINITE QW WITH A DIVERGING ASYMMETRY

As shown in Fig. 3, the maximum value of $\mu_{12}^2\delta_{12}$ is obtained for $d\to0$ and $V\to\infty$. This corresponds to a QW with an increasing and diverging asymmetry. A careful examination of our numerical results shows that this maximum is obtained when the first level E_1 is very close to V. This can be understood in the following way. If E_1 is below V, the first level is localized in the GaAs part of the QW while the second level is delocalized in the QW: μ_{12} is small and δ_{12} is large. On the other hand, if E_1 is above V, both levels are delocalized in the QW: then μ_{12} is large and δ_{12} is small. The condition $E_1=V$ corresponds to a tradeoff between both situations. We derive below the value of the dipolar matrix elements in an asymmetrical step quantum well with $E_1=V$ and $d\to0$.

The first wave function in the well is thus

$$\begin{aligned}&\zeta_{\mathrm{GaAs}}(z)=A_{\mathrm{GaAs}}\sin kz, \quad \text{for } 0<z<d\ ;\\ &\zeta_{\mathrm{Al}_x\mathrm{Ga}_{1-x}\mathrm{As}}(z)=A_{\mathrm{Al}_x\mathrm{Ga}_{1-x}\mathrm{As}}(z-L), \quad \text{for } d<z<L\ ;\end{aligned} \tag{A1}$$

where the wave vector $k=\sqrt{2m^*V}/\hbar$ is given by the continuity condition

$$\frac{\tan(kd)}{k}=d-L\ . \tag{A2}$$

Since $k\to\infty$, then $kd\to\pi/2$ in order to satisfy Eq. (A2) so that

$$V\approx\frac{\hbar^2\pi^2}{8m^*d^2}\ . \tag{A3}$$

The wave function of the second level $E_2=V+h\nu$ is

$$\begin{aligned}&\zeta_{\mathrm{GaAs}}(z)=B_{\mathrm{GaAs}}\sin(q_{\mathrm{GaAs}}z), \quad \text{for } 0<z<d\ ;\\ &\zeta_{\mathrm{Al}_x\mathrm{Ga}_{1-x}\mathrm{As}}(z)=B_{\mathrm{Al}_x\mathrm{Ga}_{1-x}\mathrm{As}}\sin[q_{\mathrm{Al}_x\mathrm{Ga}_{1-x}\mathrm{As}}(L-z)], \quad \text{for } d<z<L\ ;\end{aligned} \tag{A4}$$

with the wave vectors given by

$$\begin{aligned}q_{\mathrm{GaAs}}&=\frac{\sqrt{2m^*(V+h\nu)}}{\hbar}\ ,\\ q_{\mathrm{Al}_x\mathrm{Ga}_{1-x}\mathrm{As}}&=\frac{\sqrt{2m^*h\nu}}{\hbar}=\frac{\pi}{d_\nu}\ .\end{aligned} \tag{A5}$$

The continuity condition reads

$$\frac{\tan(q_{\mathrm{GaAs}}d)}{q_{\mathrm{GaAs}}}=-\frac{\tan[q_{\mathrm{Al}_x\mathrm{Ga}_{1-x}\mathrm{As}}(L-d)]}{q_{\mathrm{Al}_x\mathrm{Ga}_{1-x}\mathrm{As}}}\ . \tag{A6}$$

When $d\to0$, then $q_{\mathrm{GaAs}}\to k$ and therefore

$\tan q_{Al_xGa_{1-x}As}(L-d) \cong q_{Al_xGa_{1-x}As}(L-d)$ from Eq. (A2). Consequently, the limit width of the asymmetric QW is given by

$$L = \frac{\theta}{\pi} d_\nu \ , \tag{A7}$$

where θ is the smallest solution of the implicit equation $\tan\theta = \theta$, i.e., $\theta = 4.4934$. This limit is clearly seen in Fig. 3. One is left with computing the normalization factors of the wave functions. One finds, respectively, $A_{GaAs} = \sqrt{3/L}$, $A_{Al_xGa_{1-x}As} = -\sqrt{3/L^3}$, $B_{GaAs} = \sqrt{2/L}\sin\theta$, and $B_{Al_xGa_{1-x}As} = \sqrt{2/L}$. Using the wave functions of Eqs. (A1) and (A4), the overlap integral μ_{12} and the electron mean displacements can be calculated and are, respectively,

$$\mu_{12} = \frac{\sqrt{6}}{\theta^3} L \frac{(1-\cos\theta)^2}{\cos\theta} \tag{A8}$$

and $\delta_{12} = L/4$. The value of the optimal $\mu_{12}^2 \delta_{12}/L$ product, which maximizes the electro-optic coefficient, calculated under the condition $E_1 = V$ is thus finally

$$\frac{{\mu_{12}}^2 \delta_{12}}{L} = \frac{3}{2\pi^2} \frac{(1-\cos\theta)^4}{\cos^2\theta\, \theta^4} d_\nu^2 \ . \tag{A9}$$

[1] C. Weisbuch and B. Vinter, *Quantized Semiconductor Structures: Fundamentals and Applications* (Academic, Boston, 1991), pp. 1–252.

[2] L. C. West and S. J. Eglash, Appl. Phys. Lett. **46**, 1156 (1985).

[3] B. F. Levine, K. K. Choi, C. G. Bethea, J. Walker, and R. J. Malik, Appl. Phys. Lett. **50**, 1092 (1987).

[4] Y. R. Shen, *The Principles of Nonlinear Optics* (Wiley, New York, 1984).

[5] M. K. Gurnick and T. A. DeTemple, IEEE J. Quantum Electron. **QE-19**, 791 (1983).

[6] J. Khurgin, *Second-Order Intersubband Nonlinear Optical Susceptibilities of Asymmetric Quantum Well Structures* (Optical Society of America, Washington, D.C., 1989), pp. 69–72.

[7] D. Ahn and S. L. Chuang, IEEE J. Quantum Electron. **23**, 2196 (1987).

[8] M. M. Fejer, S.J.B. Yoo, R. L. Byer, A. Harwit, and J. S. Harris, Phys. Rev. Lett. **62**, 1041 (1989).

[9] P. F. Yuh and K. L. Wang, J. Appl. Phys. **65**, 4377 (1989).

[10] E. Rosencher, P. Bois, J. Nagle, and S. Delaître, Electron. Lett. **25**, 1063 (1989).

[11] E. Rosencher, P. Bois, and J. Nagle, SPIE Proc. **1273**, 138 (1990).

[12] E. Rosencher, P. Bois, B. Vinter, J. Nagle, and D. Kaplan, Appl. Phys. Lett. **56**, 1822 (1990).

[13] E. Rosencher, P. Bois, J. Nagle, E. Costard, and S. Delaître, Appl. Phys. Lett. **55**, 1597 (1989).

[14] P. Boucaud, F. H. Julien, D. D. Yang, J. M. Lourtioz, E. Rosencher, P. Bois, and J. Nagle, Appl. Phys. Lett. **57**, 215 (1990).

[15] R. P. Karunasiri, Y. J. Mii, and K. L. Wang, IEEE Electron Dev. Lett. **11**, 227 (1990).

[16] C. Flytzanis, in *Nonlinear Optical Properties of Organic Molecules and Crystals,* edited by D. S. Chemla and J. Zyss (Academic, New York, 1987), p. 121.

[17] J. L. Oudar and J. Zyss, Phys. Rev. A **26**, 2016 (1982).

[18] G. Bastard, *Wave Mechanics Applied to Semiconductor Heterostructures* (Les Editions de Physique CNRS, Paris, 1988).

[19] S. J. Allen, D. C. Tsui, and B. Vinter, Solid State Commun. **20**, 425 (1976).

[20] B. Vinter, Phys. Rev. B **26**, 6808 (1982).

[21] C. Cohen-Tannoudji, B. Diu, and F. Laloë, *Mécanique Quantique* (Hermann, Paris, 1973).

[22] R. Loudon, *The Quantum Theory of Light* (Clarendon, Oxford, 1983).

[23] E. O. Kane, J. Phys. Chem. Solids **1**, 249 (1956).

[24] A. Yariv, *Quantum Electronics,* 3rd ed. (Wiley, New York, 1989).

[25] L. Tsang, D. Ahn, and S. L. Chuang, Appl. Phys. Lett. **52**, 697 (1988).

[26] K. W. Goossen and S. A. Lyon, Appl. Phys. Lett. **47**, 1257 (1985).

[27] C. Kittel, *Introduction to Solid State Physics,* 5th ed. (Wiley, New York, 1976).

[28] A. Seilmeier, H. J. Hübner, G. Abstreiter, G. Weimann, and W. Schlapp, Phys. Rev. Lett. **59**, 1345 (1987).

[29] B. Vinter and F. Chevoir, *Resonant Tunneling: Physics and Applications,* edited by L. L. Chang (Plenum, New York, 1991).

[30] Y. J. Mii, K. L. Wang, R.P.G. Karunasiri, and P. F. Yuh, Appl. Phys. Lett. **56**, 1046 (1990).